Science of Sintering, **51** (2019) 209-221

doi:https://doi.org/10.2298/SOS1902209S

UDK: 669.018; 676.017.5

Effect of deposition current density and annealing temperature on the microstructure and magnetic properties of nanostructured Ni-Fe-W-Cu alloys

Milica Spasojević[1*)], Dušan Marković[2], Miroslav Spasojević[2], Zoran Vuković[2], Aleksa Maričić[2], Lenka Ribić-Zelenović[2]

[1]Faculty of Chemistry, University of Belgrade, Belgrade, Serbia

[2]Joint Laboratory for Advanced Materials of SASA, Section for Amorphous Systems, Faculty of Technical Sciences, Čačak, University of Kragujevac, Čačak, Serbia

Abstract:

Ni-Fe-W-Cu alloy powders were obtained by electrodeposition from an ammonium citrate bath at current densities ranging between 70 and 600 mA cm^{-2}. As the deposition current density increased, the contents of Fe and W in the alloy increased, and those of Ni and Cu decreased. The total cathodic polarization curve was recorded, and partial polarization curves for Ni, Fe and W deposition and hydrogen evolution were determined. The current efficiency of alloy deposition was measured. The powders contained an amorphous matrix and FCC nanocrystals of the solid solution of Fe, W and Cu in Ni. At high current densities, small-sized nanocrystals exhibiting high internal microstrain values were formed. Powder particles were dendrite- and cauliflower-shaped. The dendrites had a large number of secondary branches and higher-order branches containing interconnected globules. The density of branches was higher in particles formed at high current densities. The powders formed at high current densities exhibited higher magnetization. Annealing at temperatures up to 460 °C resulted in structural relaxation, accompanied by an increase in magnetization. At temperatures above 460 °C, amorphous matrix crystallization and FCC crystal growth took place, accompanied by a decrease in magnetization.

Keywords*: Nanostructured alloy; FCC phase; Powder; Magnetization; Nickel-iron-tungsten-copper alloy.*

1. Introduction

Nanostructured materials have been increasingly used in a wide range of technologies. Nanostructured nickel-iron alloys have good mechanical, electrical and magnetic properties, and demonstrate high catalytic activity for a number of chemical and electrochemical reactions [1-10]. Alloying with small amounts of tungsten improves the corrosion resistance, thermal stability, wear resistance, microhardness and high-temperature oxidation behavior of these alloys. Nickel-iron-tungsten alloys are in wide use in different industries for the fabrication of a variety of devices, such as inductor cores for electromagnets [2-4], magnetic devices [5], microwave noise filters [6], magnetic recording heads [7-9] and tunable noise suppressors [10]. They are also used as catalysts in some chemical processes and as cathodes for the electrochemical production of hydrogen [11]. The metallurgic

*) **Corresponding author:** smilica84@gmail.com

manufacture of nickel-iron-tungsten alloys is a highly expensive process since it is energy intensive due to the high melting point of tungsten. Therefore, much cheaper processes have been developed, i.e. mechanical alloying, sputtering and electrolytic deposition from environmentally friendly citrate ammonia solutions [10-25]. Electrochemical methods result in alloys which differ in chemical composition, morphology, microstructure, and mechanical, electrical, magnetic, catalytic and corrosion properties from those obtained by other techniques. The properties of electrodeposited metals and alloys are dependent on the temperature, pH and composition of the solution, current density, cathode material and cathodic diffusion layer thickness [12, 14, 19, 22, 26-30].Tungsten and molybdenum can be co-deposited from aqueous solutions with iron-group metals [12, 31-33]. The kinetics and mechanism of co-deposition of these metals have been analyzed in a number of studies [31-37].

Nanostructured metals and alloys are in a metastable state. Their annealing at elevated temperatures induces changes in their microstructure, leading to changes in their physical and chemical properties [12-22, 38-40]. Annealing nanostructured alloys at temperatures below the crystallization temperature causes short-range ordering, whereas amorphous phase crystallization and nanocrystalline grain growth occur at higher temperatures. These structural changes affect mechanical, electrical and magnetic properties, catalytic activity, thermal stability and corrosion resistance [12-22, 38-40].

Many specifically shaped components of devices used in industries, agriculture and medicine are obtained from sintered powders of nickel-iron-tungsten alloys. This is a simple and low-cost procedure which requires minimum investments.

Nanostructured nickel-iron-tungsten alloy powders having desired chemical compositions, microstructures, particle sizes and particle shapes cannot be produced from an ammonium citrate bath at high current efficiencies [16, 18, 21].

The deposition of nickel, iron and tungsten along with a small amount of copper from environmentally friendly citrate ammonia solutions at high current densities with high current efficiencies can result in desired physical and chemical properties and the desired particle size and shape, without any environmental and health risks [16, 18].

The objective of this study was to investigate the effect of current density for the deposition of nickel-iron-tungsten alloy powders containing small amounts of copper from an ammonium citrate bath on their chemical composition, morphology, microstructure and magnetic properties. Moreover, the experimental research aimed to assess the effect of annealing of these alloys at different temperatures on their microstructure and magnetization.

2. Materials and Experimental Procedures

Nickel-iron-tungsten-copper alloys were deposited in a 2.0 dm^3 glass electrochemical cell. A Lugin capillary and a saturated calomel electrode were placed in a separate compartment of the cell. A 12 cm^2 Pt plate was used as the anode. A 4 cm^2 titanium plate cathode was placed parallel to the anode at a distance of 0.7 cm. The cell-containing thermostat was used to regulate the operating temperature at 60±0.5 ^oC. The electrodeposition of the alloys and electrochemical measurements were performed using a standard electrical circuit comprising a potentiostat equipped with a programmer (Potentiostat-Galvanostat model 173, EG G Princeton, Applied Research, Princeton, USA), an x-y recorder (Hewlett Packard 7035 B) and a voltmeter (Pro's Kit 03-9303 C). Electrolysis was carried out in a bath containing 0.2 mol dm^{-3} $NiSO_4$, 0.02 mol dm^{-3} $FeSO_4$, 0.04 mol dm^{-3} Na_2WO_4, 0.005 mol dm^{-3} $CuSO_4$, 0.24 mol dm^{-3} $Na_3C_6H_5O_7$ (Na_3Cit), 0.8 mol dm^{-3} NH_4Cl and 0.3 mol dm^{-3} Na_2SO_4. During the experiment, the pH of the solution was 9.2±0.1, and was maintained by adding 0.6 mol dm^{-3} NH_4OH to the bath. The solution was made up from p.a. chemicals (Merck). The potentials were expressed relative to S.H.E. They were corrected for the ohmic potential drop

which was determined by the galvanostatic pulse method. After the electrolysis, the resulting powder was washed three times with distilled water and with a 0.1 wt.% solution of benzoic acid to prevent oxidation. Thereafter, it was dried at 105 ^{o}C. The current efficiency of Ni-Fe-W-Cu alloy deposition was determined by measuring the weight of the deposited alloy and the rate of hydrogen evolution. The time taken for the graduated burette, located above the titanium cathode, to fill with the evolved hydrogen was measured.

A Pektar-A-200-Varian atomic absorber was used to determine the chemical composition of the powder. The distribution of minimum and maximum particles sizes was determined by a Leica Q500 MC automatic device for microstructural analysis. Scanning electron microscopy (SEM) analysis was performed by a JEOL-JSM 5300. X-ray diffraction (XRD) was recorded by a Philips PW 1710 diffractometer using CuKα radiation (λ= 0.154 nm) and a graphite monochromator. XRD data were collected with a step size of 0.03° and a collection time of 1.5 s step^{-1}.

Thermomagnetic measurements were performed by a modified Faraday method based on the effect of an inhomogeneous magnetic field on the magnetic sample. The magnetic field strength (H) at the sample location was 10 kAm^{-1}. Magnetic force measurements were carried out with a sensitivity of 10^{-6} N in an argon atmosphere.

3. Results and Discussion

Nickel-iron-tungsten-copper alloy powders were deposited on the titanium cathode at current densities of 70 mA cm^{-2}, 200 mA cm^{-2}, 400 mA cm^{-2} and 600 mA cm^{-2} from an ammonium citrate bath. Powder samples were collected for analysis from parts of powders deposited only after thirty minutes of electrolysis. All deposits were black. The chemical composition of the powders was determined by atomic absorption analysis. The average composition of the alloys, resulting from five analyses of the same sample, is presented in Table I and Figure 1.

Tab. I The chemical composition of nickel-iron-tungsten-copper alloy powders as a function of electrodeposition current density.

j (mA cm^{-2})	70	200	400	600
Ni (wt.%)	86.70	86.30	86.00	85.77
Fe (wt.%)	5.66	8.27	9.80	10.63
W (wt.%)	0.74	1.03	1.30	1.40
Cu (wt.%)	6.90	4.40	2.90	2.20

Figure 1. shows an increase in Fe and W contents in the alloy from 70 to 400 mAcm^{-2} and a decrease in Ni and Cu contents. At current densities above 400 mAcm^{-2}, there is the same trend of changes, but at a considerably lower rate.

Figure 2. shows the total cathodic polarization curve and partial polarization curves for Ni, Fe and W deposition and hydrogen evolution. The same figure also presents the current efficiency for Ni, Fe, W and Cu deposition as a function of current density. When recording the polarization curves and measuring the current efficiency, the alloy was first deposited for 30 minutes at j = 600 mAcm^{-2}, and then the current density was changed to the specified value. Then, after 40 s, the potential value was recorded, and the time taken for the burette to fill with the evolved hydrogen was measured. Thereafter, the current density was again changed to j = 600 mAcm^{-2}. After five minutes of electrolysis at j = 600 mAcm^{-2}, the current density was again changed to another specified value. The deposition of the alloy for five minutes at j = 600 mAcm^{-2} and the recording of the potential after 40 s of electrolysis at the specified current density were repeated until the total polarization curve was recorded and

the cathodic current efficiency of the deposited alloy determined. This polarization curve recording method ensures that the real surface area of the cathode during the recording is not considerably changed. At current densities above 20 $mAcm^{-2}$, Cu is deposited from the solution through the limit diffusion current [18]. Based on this fact and on the Cu content in the alloy deposited at j = 600 $mAcm^{-2}$, the limit diffusion current for copper deposition was determined. Then, based on the total polarization curve, partial limit diffusion currents for Cu deposition and current efficiency of alloy deposition, the partial currents for Ni, Fe and W deposition and hydrogen evolution were determined (Figure 2).

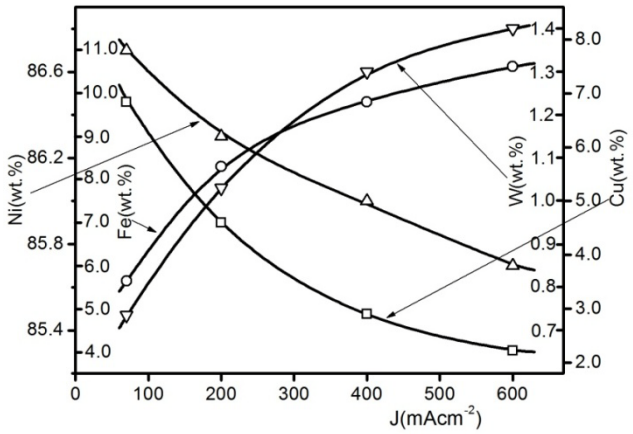

Fig. 1. The chemical composition of nickel-iron-tungsten-copper alloy powders as a function of electrodeposition current density: Δ - Ni; ○ – Fe; ∇ - W and □ – Cu.

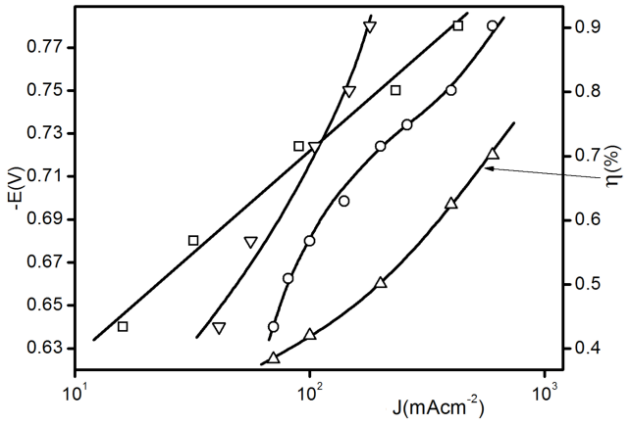

Fig. 2. Cathodic polarization curve: ○ – total cathodic polarization curve; □ – polarization curve for Ni, Fe and W deposition, ∇- polarization curve for hydrogen evolution, and Δ - current efficiency for alloy deposition as a function of the potential.

The partial polarization curve for Ni, Fe and W deposition shows that the deposition of these metals in the partial current density range of 17 – 400 $mAcm^{-2}$ is an activation-controlled process with a Tafel slope of 115 mV. It was shown that, at potentials more positive than -0.9 V, hydrogen is evolved from NH_4^+ and $(HCit)^{3-}$ ions from an ammonium citrate bath at pH = 9.2 [18, 21, 27, 34, 41]. The shape of the polarization curve (Figure 2) indicates that, in the potential range of 0.64 – 0.78 V, hydrogen evolution is both activation- and diffusion-controlled. This finding is supported by the appearance of a current wave on the total polarization curve in the current density range of 70 – 200 $mAcm^{-2}$, and the fact that, in this range, the current density of the alloy current efficiency decreases with an increasing rate

of mixing of the solution with the inert gas, as induced by the increase in hydrogen evolution rate due to the reduction in diffusion layer thickness.

SEM micrographs show that deposition results in dendritic particles (Figure 3a) and cauliflower-shaped particles (Figure 3b).

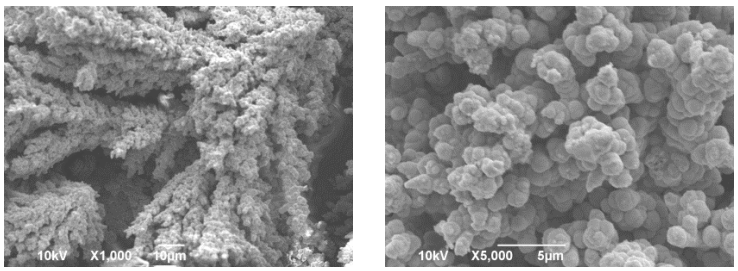

a) b)

Fig. 3. SEM micrographs of Ni-Fe-W-Cu alloy powders electrodeposited at the current density of 70 mAcm^{-2}.

The dendritic particles deposited at all current densities (70, 200, 400, 600 mAcm^{-2}) exhibit a high density of secondary and higher-order branches. The high density of branches is caused by high cathodic polarization at operating current densities and by copper and tungsten co-deposition [18]. As the polarization increases, the critical radius of the nucleus, the number of atoms in the critical nucleus and the induction period are decreased. Therefore, at high current densities, the rate of nucleation is higher and the surface density of nuclei is greater. Many of these nuclei are branch initials; therefore, the density of branches increases with increasing polarization. The overpotential of copper deposition at the operating current density for alloy deposition is high, and hence the co-deposition of copper with Ni, Fe and W substantially enhances the formation of nuclei. Therefore, the number of secondary and higher-order branches is considerably greater in Ni-Fe-W alloy particles containing a small amount of Cu than in those without copper. The increase in W content in the alloy with increasing current density indirectly promotes the formation of new nuclei. Namely, considerably greater W adatoms are difficult to embed into existing crystalline grains of the alloy. This decreases the crystal growth rate and creates more favorable conditions for nuclei formation. Figures 3. and 4. show that the branches are made up of a series of merged globules.

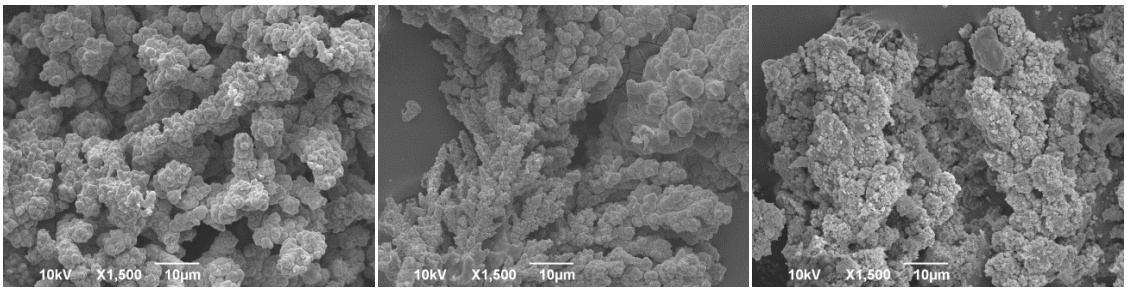

a) b) c)

Fig. 4. SEM micrographs of Ni-Fe-W-Cu alloy powder electrodeposited at current densities: a) 200 mAcm^{-2}; b) 400 mAcm^{-2} and c) 600 mAcm^{-2}.

Nuclei are formed on branches, where they turn into globules. As the result of fast nucleation, these globules, before they turn into a large crystal, serve as sites for further nuclei formation. The new nuclei formed on the tips and lateral sides of globules also turn into globules over time. This formation of new globules continues, leading to the formation of both main and

lateral branches made up of a series of merged globules. Once the density of branches reaches the critical value, globules merge on the particle surface to create a cauliflower (Figures. 3 and 4). Then, new globules are formed on the cauliflower surface (Figures. 3b, 4a, 4b and 4c). At higher current densities, the higher nucleation rate causes a greater branch density and, hence, smaller merged globules on the cauliflower surface (Figure. 4). This mechanism of cauliflower particle formation shows why smaller jagged particles of considerably higher specific surface area are formed at higher current densities. Due to higher internal microstrain, a larger number of cracks occur in the deposit formed at higher current densities, which additionally increases its specific surface area (Figure. 5). Also, in some parts of the deposit, craters i.e. sites of hydrogen bubble evolution are observed. On the surface below hydrogen bubbles, alloy deposition was not possible.

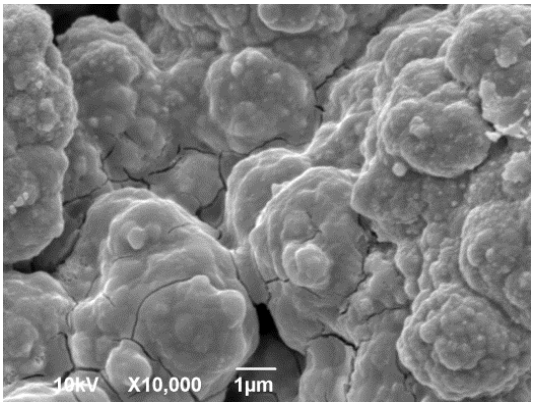

Fig. 5. SEM micrographs of Ni-Fe-W-Cu alloy powder electrodeposited at the current density of 400 mAcm^{-2}.

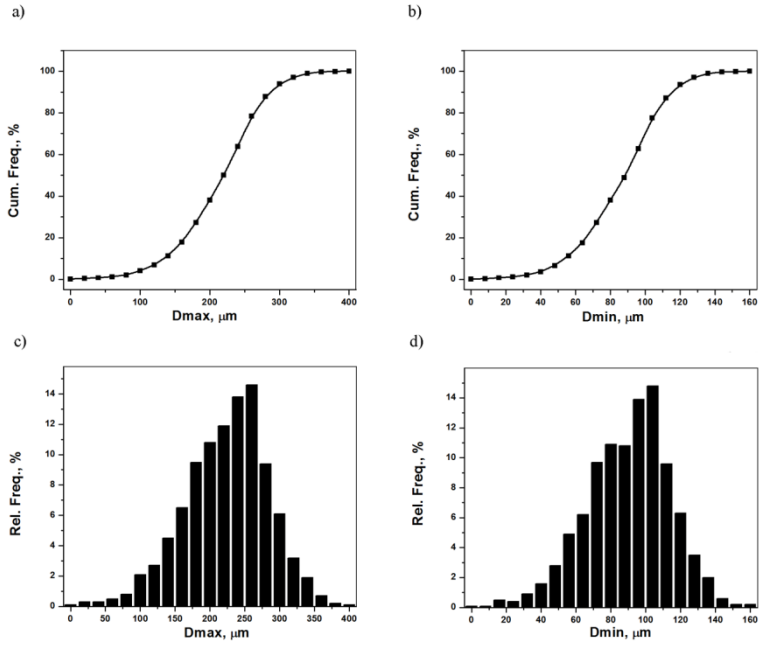

Fig. 6. Cumulative particle size distribution curves of: a) maximum particle size D_{max}, b) minimum particle size, D_{min}, and c) histograms of relative frequencies of maximum particle size, D_{max} and d) minimum particle size, D_{min}, of Ni-Fe-W-Cu alloy powder deposited at j = 70 mAcm^{-2}.

The above considerations indicate that the real surface area of the cathode increases with increasing geometric current density. The values of the content of Cu deposited under limiting diffusion current conditions and the polarization curves (Figure. 2) obtained at an approximately constant value of the real surface area were used to determine the ratio of geometric surfaces of the cathode at different current densities: $S_{600} = 1.25 \cdot S_{70}$; $S_{400} = 2.0 \cdot S_{70}$; $S_{200} = 3.3 \cdot S_{70}$.

The size and shape of the deposited Ni-Fe-W-Cu alloy particles are dependent on deposition current density [17, 18]. The cumulative curves of maximum and minimum particle size distribution and histograms of relative frequencies of maximum and minimum particle sizes of Ni-Fe-W-Cu alloy powders obtained at j = 70 mAcm^{-2} (Figure. 6), j = 200 mAcm^{-2}, j = 400 mAcm^{-2} (Figure. 7) and j = 600 mAcm^{-2} show that the average size of particles decreases and their roundness increases with increasing deposition current density.

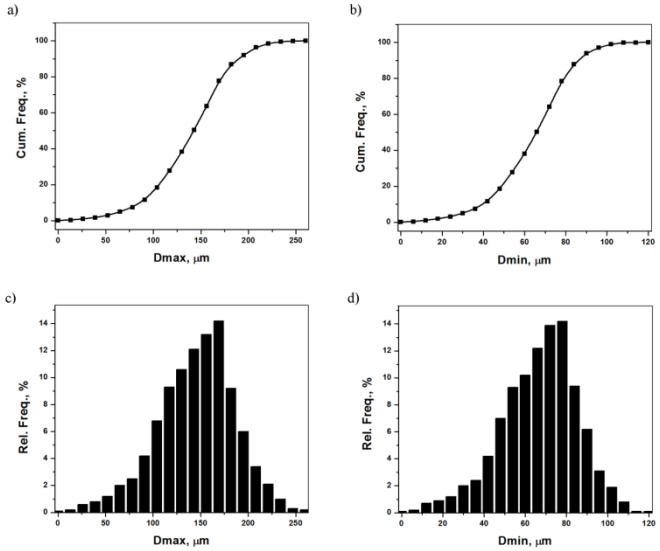

Fig. 7. Cumulative particle size distribution curves of: a) maximum particle size D_{max}, b) minimum particle size, D_{min}, and c) histograms of relative frequencies of maximum particle size, D_{max} and d) minimum particle size, D_{min}, of Ni-Fe-W-Cu alloy powder deposited at j = 400 mAcm^{-2}.

The phase structure of Ni-Fe-W-Cu alloy powders obtained by electrodeposition at different current densities was determined by XRD analysis (Figure. 8).

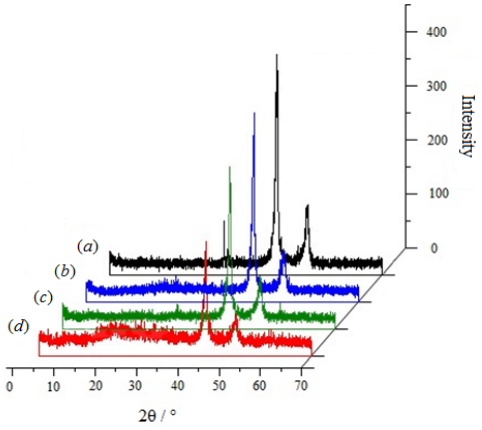

Fig. 8. XRD pattern of as-deposited Ni-Fe-W-Cu alloys obtained at current densities: a) 70 mAcm^{-2}; b) 200 mAcm^{-2}; c) 400 mAcm^{-2} and d) 600 mAcm^{-2}.

As shown, XRD patterns of powders contain only peaks for the (111) and (200) planes of the FCC solid solution of iron, tungsten and copper in nickel. There are no clearly pronounced peaks for either pure metals, their intermetallic compounds or metal oxides. The ratio of the relative integral intensity of (111) peak to that of (200) peak was the same in all four samples tested. The same value of this ratio was found for the untextured nickel polycrystal. This indicates that there is no preferred growth along the specified orientation and that the strain is distributed in different directions as in the randomly textured nickel polycrystal. The sum of integrals of (111) and (200) relative peak intensities decreases from the sample obtained at the highest current density to the sample deposited at the lowest current density. This indicates that the increase in electrodeposition current density results in deposits containing a substantial proportion of the amorphous phase, and that the deposit comprises an amorphous matrix with embedded crystalline grains of the FCC solid solution. Peak maxima are shifted to lower 2θ values relative to the maximum 2θ values of the FCC phase of pure nickel. This shift is more pronounced in powders obtained at higher current densities. The crystalline grains of all electrodeposited powders are relatively small in size, and have high mean internal microstrain values (Table II).

Tab. II Microstructural data for Ni-Fe-W-Cu alloy powders as dependent on electrodeposition current density.

Current density ($mAcm^{-2}$)	**Mean crystallite size (nm)**	**Mean microstrain value**
70	17 (3)	$1.0\ (3) \cdot 10^{-3}$
200	14 (3)	$1.2\ (3) \cdot 10^{-3}$
400	12 (3)	$1.4\ (4) \cdot 10^{-3}$
600	10.6 (3)	$1.6\ (4) \cdot 10^{-3}$

The results in Table II show that the mean size of nanocrystals decreases and the mean value of internal microstrain increases with increasing current density.

The ensuing microstructure is determined by the electrodeposition current density and the contents of iron, copper and tungsten in the nickel alloy [12-22, 26]. Current density has both an indirect and a direct effect [15, 17, 20, 21]. The direct effect is related to the increase in nucleation rate as induced by increasing current density. Faster nucleation causes the formation of small crystal grains exhibiting high internal microstrain and a high density of chaotically distributed dislocations. As the mean size of nanocrystals decreases, the proportion of the amorphous matrix in the electrodeposit increases [17, 19, 26, 42]. The indirect effect of current density is produced through its effect on the alloy composition. The iron, copper and tungsten present in the solid solution of the FCC phase of nickel increase the interatomic distance in the crystal lattice, thus causing its deformation. This hampers crystalline grain growth [12-22, 26], as manifested by a shift in peak maxima to lower 2θ values.

In these electrodeposited alloys, the largest contribution is made by W atoms as they are much larger than atoms of the other metals.

The magnetic properties of the electrodeposited Ni-Fe-W-Cu alloy powders are dependent on their microstructure and chemical composition. Annealing the nanostructured powders at elevated temperatures induces changes in their microstructure, leading to changes in their magnetic properties [15, 21, 29, 30, 33]. Figures 9a-d show: a) temperature-dependent magnetization, M_t, of as-deposited powders, b) magnetization, M_{20}, of powders cooled at 20 °C as a function of annealing temperature, and c) temperature-dependent magnetization, M_{460}, of powders annealed at 460 °C.

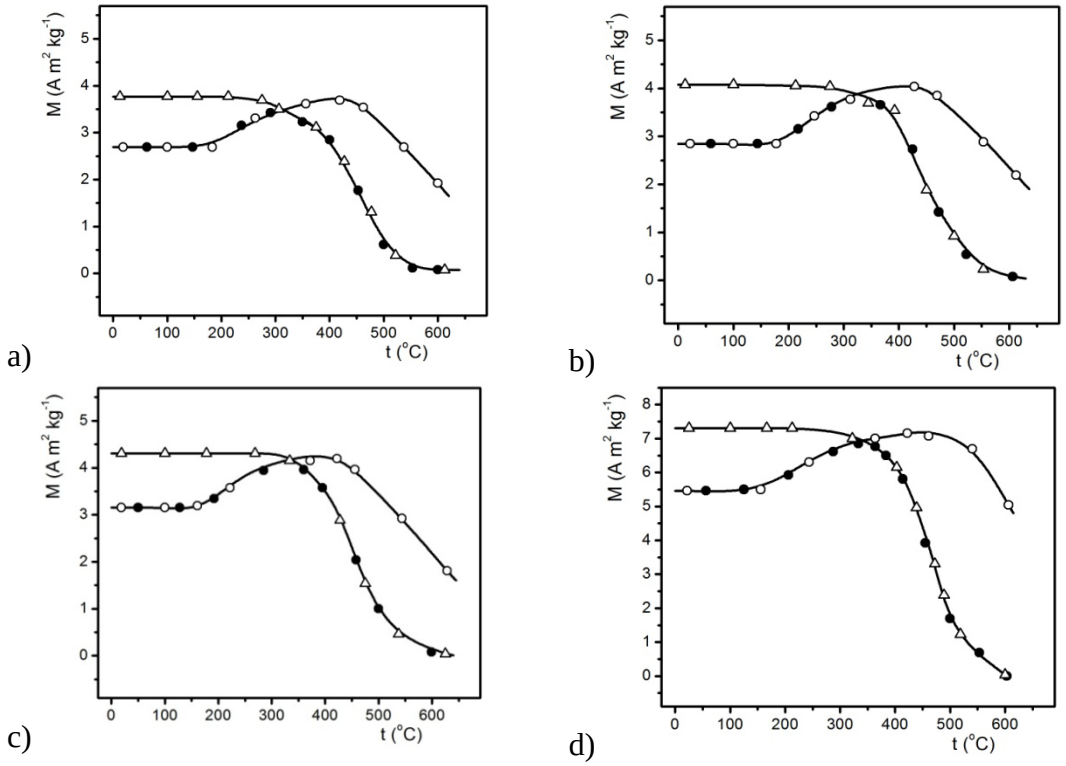

Fig. 9. ● – temperature-dependent magnetization, M_t, of as-deposited powders, ○ – magnetization, M_{20}, of powders cooled at 20 °C as a function of annealing temperature, and Δ – temperature-dependent magnetization, M_{460}, of powders annealed at 460 °C. The powders were electrodeposited at current densities of: a) 70 mAcm^{-2}; b) 200 mAcm^{-2}; c) 400 mAcm^{-2}, and d) 600 mAcm^{-2}.

The plot of the temperature-dependent magnetization, M_t, of as-deposited powders and that of the magnetization of powders cooled to 20 ^oC, M_{20}, as a function of annealing temperature show no change in the magnetization of powders during heating at temperatures between 20 ^oC and t_s. This indicates that no structural change takes place in as-deposited powders during annealing in this temperature range. The temperature t_s is dependent on deposition current density. As the current density increases, the stability temperature, t_s, of as-deposited powders decreases. At j = 70 mAcm^{-2}, t= 180 ^oC; at j = 200 mAcm^{-2}, t_s = 170 ^oC; at j = 400 mAcm^{-2}, t_s = 160 ^oC, and at j = 600 mAcm^{-2}, t_s = 150 ^oC. The powders obtained at high current densities have small crystalline grains exhibiting a higher density of chaotically distributed dislocations and higher internal microstrain. Therefore, these powders require less heat for structural relaxation to start. When heating the as-deposited powders in the temperature range of t_s to 360 ^oC, the increase in temperature induces an increase in their magnetization, M_t. However, as the temperature of these powders is further increased from 360 to 400 ^oC, the magnetization, M_t, gradually decreases, followed by an abrupt decrease at temperatures ranging from 400 to 500 ^oC. This decrease is due to the heat-induced reorientation of magnetic domains. However, the plot of the magnetization of samples cooled at 20 ^oC as a function of annealing temperature shows that the magnetization, M_{20}, increases with increasing annealing temperature in the temperature range between t_s and 460 ^oC. The XRD patterns of alloys annealed in this temperature range are congruous with those of as-deposited alloys. This congruity indicates that, during annealing of as-deposited powders in the temperature range t_s–460 ^oC, neither amorphous phase crystallization nor FCC crystalline grain growth occurs in alloys obtained at current densities of 70 – 600 mAcm^{-2}. The increase

in the magnetization of these samples cooled at 20 °C is due to structural relaxation [15, 21, 29, 30, 33]. During annealing at temperatures ranging from t_s to 460 °C, both the amorphous phase and the nanocrystals of the as-deposited alloy undergo short-range ordering, accompanied by decreases in the density of chaotically distributed dislocations and internal microstrain values [15, 21, 29, 30, 33]. The increase in short-range ordering enhances the mobility of magnetic domain walls and facilitates the orientation of magnetic domains in the external magnetic field, thus causing their further expansion and, hence, increases in the magnetization, M_{20} [15, 21, 29, 30, 33].

At temperatures above 460 °C, the increase in annealing temperature results in a decrease in the magnetization, M_{20}, of electrodeposited Ni-Fe-W-Cu alloy samples cooled at 20 °C. The decrease in magnetization is due to amorphous phase crystallization and the formation of considerably larger crystalline grains of the FCC solid solution of Fe, W and Cu in Ni. Large crystalline grains hamper the orientation of some magnetic domains and reduce the shift of oriented domain walls [15, 21, 29, 30, 33]. The formation of large crystalline grains and the crystallization of the amorphous phase were confirmed by the XRD patterns of the alloys annealed at 600 °C. Figure. 10. shows the XRD pattern of Ni-Fe-W-Cu alloy obtained at j = 400 mAcm^{-2} and annealed for 60 minutes.

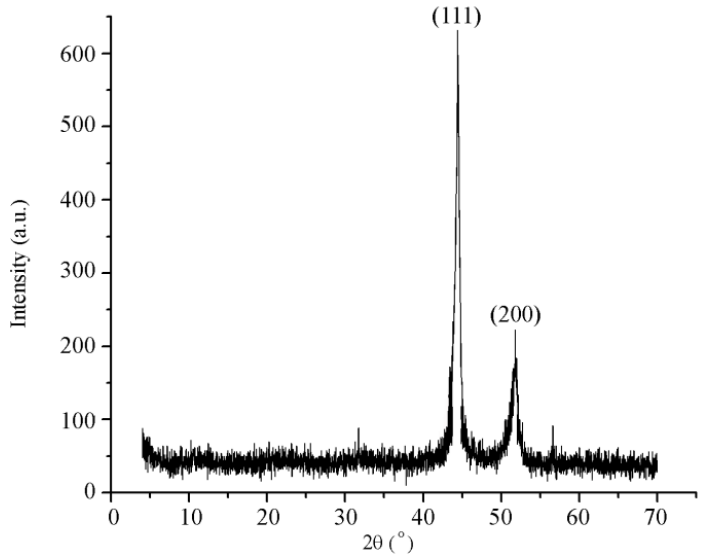

Fig. 10. XRD patterns of the alloy obtained at j = 400 mAcm^{-2} and annealed for 60 minutes at 600 °C.

The XRD patterns of the samples annealed at 600 °C have higher relative intensity integrals of the (111) and (200) peaks, higher peak intensities and smaller half-height widths compared to the XRD patterns of the as-deposited samples. The average crystallite size of the powders obtained at j = 400 mAcm^{-2} and annealed for 60 minutes at 600 °C was 29(3) nm, and the mean internal microstrain value was $0.1 \cdot 10^{-3}$ (3).

The temperature dependences of the magnetization, M_{460}, of the samples annealed at 460 °C show that the Ni-Fe-W-Cu alloys electrodeposited at current densities of 70 – 600 mAcm^{-2} from an ammonium citrate bath are magnetically stable at temperatures up to 360 °C, and that their magnetization increases with increasing electrodeposition current density.

The results show that, in the presence of complex copper ions, nanostructured Ni-Fe-W-Cu alloy powders obtained from an ammonium citrate solution at high current efficiencies exhibit good magnetic characteristics and high magnetic stability at temperatures up to 360 °C and high structural stability at temperatures up to 460 °C.

4. Conclusion

Nickel-iron-tungsten-copper alloy powders were deposited on a titanium cathode from an ammonium citrate bath at current densities ranging between 70 and 600 $mAcm^{-2}$.

As the deposition current density increases, the contents of Fe and W in the alloy increase, and those of Ni and Cu decrease.

The total cathodic polarization curve and partial polarization curves for Ni, Fe and W deposition and hydrogen evolution were recorded. The current efficiency of alloy deposition was determined.

The deposition of Ni, Fe and W is an activation-controlled process, and that of copper a diffusion-controlled process. Hydrogen is evolved from NH_4^+ and $(HCit)^{3-}$ ions under mixed activation-diffusion control.

The powders obtained at current densities ranging from 70 to 600 $mAcm^{-2}$ comprise an amorphous matrix with embedded nanocrystals of the FCC solid solution of Fe, W and Cu in nickel. As the deposition current density increases, the mean size of nanocrystals decreases and internal microstrain values increase.

Powder particles are dendrite- and cauliflower-shaped. At higher deposition current densities, small-sized particles are formed, and the dendrites have a larger number of secondary and higher-order branches made up of merged globules.

The increase in deposition current densities leads to an increase in the magnetization of powders. Annealing at temperatures up to 460 ^oC causes short-range ordering in the powders, resulting in an increase in their magnetization. At temperatures above 460 ^oC, amorphous matrix crystallization and FCC crystalline grain growth take place, accompanied by a decrease in the magnetization of the alloy.

Acknowledgments

This study was financially supported by the Ministry of Education and Science of the Republic of Serbia through Project Ref. No. 172057.

5. References

1. S. Steeb and H. Warlimont, Rapidly Quenched Metals, Elsevier, Amsterdam (1985).
2. T. O'Donnell, N. Wang, S. Kulkarni, R. Meere, F. M. F. Rhen, S. Roy, and S. C. O'Mathuna, J. Magn. Magn. Mater., 322, 1690 (2010).
3. E. Kubo, N. Ooi, H. Aoki, D. Watanabe, J. H. Jeong, C. Kimura, and T. Sugino, Jpn. J. Appl. Phy., 49, 04DB17 (2010).
4. T. Dastagir, W. Xu, S. Sinha, H. Wu, Y. Cao, and H. Yu, Appl. Phys. Lett., 97, 162506 (2010).
5. O. Song, C. A. Ballentine, and R. C. O'Handley, Appl. Phys. Lett., 64, 2593 (1994).
6. C. Jiang, D. Xue, and W. Sui, Thin Solid Films, 519, 2527 (2011).
7. E. I. Cooper, C. Bonhote, J. Heidmann, Y. Hsu, P. Kern, J. W. Lam, M. Ramasubramanian, N. Robertson, L. T. Romankiw, and H. Xu, IBM J. Res. Dev., 49, 103 (2005).
8. B. Koo and B. Yoo, Surf. Coat. Tech., 205, 740 (2010).
9. T. Osaka, T. Asahi, J. Kawaji, and T. Yokoshima, Electrochim. Acta, 50, 4576 (2005).
10. B. K. Kuanr, R. Marson, S. R. Mishra, A. V. Kuanr, R. E. Camley, and Z. J. Celinski, J. Appl. Phys., 105, 07A520 (2009).

11. M. A. Oliver-Tolentino, E. M. Arce-Estrada, C. A. Cortés-Escobedo, A. M. Bolarín-Miro, F. Sánchez-De Jesús, R. de G. González-Huerta, and A. Manzo-Robledo, J. Alloys Comp., 536, S245 (2012).
12. M. Donten, H. Cesiulis, and Z. Stojek, Electrochim. Acta, 45, 3389 (2000).
13. S. J. Mun, M. Kim, T. H. Yim, J. H. Lee, and T. Kang, J. Electrochem. Soc., 157, D177 (2010).
14. F. He, J. Yang, T. Lei, and C. Gu, Appl. Surf. Sci., 253, 7591 (2007).
15. M. Spasojević, N. Ćirović, L. Ribić-Zelenović, P. Spasojević, and A. Maričić, J. Electrochem. Soc., 161, D463 (2014).
16. Z. Vuković, P. Spasojević, M. Plazinić, J. Živanić, and M. Spasojević, J. Optoelectron. Adv. M., 16, 985 (2014).
17. N. Ćirović, P. Spasojević, L. Ribić-Zelenović, P. Mašković, and M. Spasojević, Sci. Sinter., 47, 347 (2015).
18. M. Spasojević, D. Gospavić, and M. Spasojević, J. Electrochem. Soc., 163, D842 (2016).
19. K. R. Sriraman, S. Ganesh Sundara Raman and S. K. Seshadri, Mater. Sci. Tech., 22, 14 (2006).
20. L. Ribić-Zelenović, N. Ćirović, M. Spasojević, N. Mitrović, A. Maričić, and V. Pavlović, Mater. Chem. Phys., 135, 212 (2012).
21. M. Spasojević, L. Ribić-Zelenović, A. Maričić, and P. Spasojević, Powd. Tech., 254, 439 (2014).
22. P. Esther, C. Joseph Kennady, P. Saravanan, and T. Venkatachalam, J. Non-Oxide Glasses, 1, 301 (2009).
23. S. H. Hong and H. J. Ryu, Mater. Sci. Eng: A, 344, 253 (2003).
24. Z. W. Zhang, J. E. Zhou, S.Q. Xi, G. Ran, and P. L. Li, Mater. Sci. Eng: A, 379, 148 (2004).
25. Z. W. Zhang, J. E. Zhou, S. Q. Xi, G. Ran, P.L. Li, and W. X. Zhang, J. Alloys Compd., 370, 186 (2004).
26. K. R. Sriraman, S. Ganesh Sundara Raman, and S. K. Seshadri, Mater. Sci. Eng: A, 418, 303 (2006).
27. M. Banerjee, A. Singh, A. K. Majumdar and A.K. Nigam, J. Phys. Condens. Matter., 23, 306004 (2011).
28. L. Ribić-Zelenović, M. Spasojević, and A. Maričić, Mater. Chem. Phys., 115, 347 (2009).
29. L. Ribić-Zelenović, M. Spasojević, A. Maričić, and M. M. Ristić, Sci. Sinter., 41, 175 (2009).
30. N. Ćirović, P. Spasojević, L. Ribić-Zelenović, P. Mašković, A. Maričić, and M. Spasojević, Sci. Sinter., 48, 1 (2016).
31. E. J. Podlaha and D. Landolt, J. Electrochem. Soc., 143, 893 (1996).
32. A. Maričić, M. Spasojević, L. Rafailović, V. Milovanović, and L. Ribić-Zelenović, Mater. Sci. Forum, 453, 411 (2004).
33. L. Ribić-Zelenović, L. Rafailović, M. Spasojević, and A. Maričić, Phy. B, 403, 2148 (2008).
34. E. Chassaing, K. Vu Quang, and R. Wiart, J. Appl. Electrochem., 19, 839 (1989).
35. O. Younes and E. Gileadi, Electrochem. Solid-State Lett., 3, 543 (2000).
36. O. Younes, L. Zhu, Y. Rosenberg, Y. Shacham-Diamand and E. Gileadi, Langmuir, 17, 8270 (2001).
37. M.D. Obradović, R.M. Stevanović, and A.R. Despić, J. Electroanal. Chem., 552, 185 (2003).
38. M. Spasojević, L. Ribić-Zelenović, N. Ćirović, P. Spasojević, and A. Maričić, Sci. Sinter., 44, 197 (2012).
39. M. Spasojević, Milica Spasojević, A. Maričić, S. Randjić, Sci. Sinter., 48, 343 (2016).

40. N. Labus, Z. Vasiljević, O. Aleksić, M. Luković, S. Marković, V. Pavlović, S. Mentus, M. V. Nikolić, Sci. Sinter., 49, 455 (2017).
41. D. W. Ernst, R. F. Amlie, and M. L. Holt, J. Electrochem. Soc., 102, 461 (1955).
42. T. Yamasaki, Scripta Mater., 44, 1497 (2001).

Садржај: *Из амонијачно-цитратног купатила на густинама струје од 70 mAcm^{-2} до 600 mAcm^{-2}, на титанској основи депоновани су прахови легура никла, гвожђа, волфрама и бакра. Установљено је да са порастом густине струје депозиције садржај Fe и W у легури расте, док садржај Ni и Cu опада. Одређена је укупна катодна и парцијалне поларизационе криве депозиције Ni, Fe и W и реакције издвајања водоника и искоришћење струје по легури. Депозиција Ni, Fe и W је активационо а бакра дифузно контролисани процес. Водоник се издваја из NH^{4+} $(HCit)^{3-}$ јона у мешовитој активационо-дифузионој контроли.*

Прахови добијени у области густина струје од 70 mAcm^{-2} до 600 mAcm^{-2} се састоје од аморфне матрице у којој су углављени нанокристали FCC фазе чврстог раствора Fe, W и Cu у никлу. Са порастом густине струје депозиције опада средња димензија нанокристала а расту унутрашња микронапрезања.

Честице праха су облика карфиола и дендрита. На већим густинама струје депозиције настају ситније честице праха а дендрити имају више секундарних грана и грана вишег реда сатканих од међусобно спојених глобула.

Са порастом густине струје депозиције расте магнетизација прахова. Одгревањем прахова, на температурама до 460 ^{o}C у праховима се одвија уређење структуре на кратко што узрокује повећање њихове магнетизације. На температурама вишим од 460 ^{o}C кристалише аморфна матрица и расту кристална зрна чврстог раствора FCC фазе уз смањење магнетизације легуре.

Кључне речи*: Наноструктурне легуре, FCC фаза, прах, магнетизација, никал-гвожђе-волфрам-бакар легуре.*